

Multiferroic nematic d -wave altermagnetism driven by orbital-order on the honeycomb lattice

Luigi Camerano,¹ Adolfo O. Fumega,² Jose L. Lado,² Alessandro Stroppa,³ and Gianni Profeta^{1,3}

¹*Department of Physical and Chemical Sciences,
University of L'Aquila, Via Vetoio, 67100 L'Aquila, Italy*

²*Department of Applied Physics, Aalto University, 02150 Espoo, Finland*

³*CNR-SPIN L'Aquila, c/o Department of Physical and Chemical Sciences,
University of L'Aquila, Via Vetoio, 67100 L'Aquila, Italy*

Altermagnets provide promising platforms for unconventional magnetism, whose controllability would enable a whole new generation of spintronic devices. While a variety of bulk altermagnets have been discovered, altermagnetism in two-dimensional van der Waals materials has remained elusive. Here we demonstrate that the strained honeycomb monolayer VCl_3 is an orbital-order-driven ferroelectric altermagnet, exhibiting a significant and switchable spin-splitting. By using low-energy Hamiltonian and first-principles methods in combination with symmetry analysis, we reveal a unique anti-ferro-orbital-antiferromagnetic phase characterized by a 2D nematic d -wave altermagnetic spin splitting, tightly coupled with an orbital-ordered induced ferroelectric polarization. Finally, through symmetry mode analysis, we investigate how structural distortions favor the intricate interplay between orbital, altermagnetic, and ferroelectric degrees of freedom. Our study identifies VCl_3 as a prototypical 2D orbital-order-driven multiferroic altermagnet on the honeycomb lattice, establishing a van der Waals monolayer featuring altermagnetic ferroelectricity.

Multiferroic materials, defined by the coexistence and the possible coupling of multiple ferroic orders [1], offer a unique platform for functional properties, enabling the control of multiple degrees of freedom (charge, spin, lattice) through external factors. This potential is further enhanced by the remarkable tunability of two-dimensional (2D) van der Waals materials through strain, stacking, and twisting, enabling the creation of exotic phenomena such as unconventional superconductivity [2–4], heavy fermion Kondo systems [5, 6], quantum spin liquid states [7–10], and 2D multiferroicity [11–17]. Altermagnetism has emerged as a fascinating new class of antiferromagnetic order, characterized by non-relativistic spin-splitting of electronic bands in momentum space, even in materials composed of light elements [18–20], while maintaining zero net magnetization. This unique property combines features of both ferromagnetism and antiferromagnetism in a single material, offering unique opportunities for spintronics and quantum materials research. Clearly, the possibility to manipulate the spin properties of an altermagnet with electricity is particularly attractive because electric fields are much easier to manipulate and integrate into modern electronic devices than magnetic fields. Electrical tuning is potentially also faster (subnanosecond) and could use less energy, two crucial properties for the development of high-speed, low-power spintronic devices. Recently, a novel Ferroelectric Switchable Altermagnetism (FSA) has been theoretically proposed, where the reversal of ferroelectric polarization is coupled to the switching of altermagnetic spin splitting [18, 21–23]. Altermagnetism arises in fully compensated magnets where the joint parity and time-reversal (\mathcal{PT}) and $\mathcal{T}\tau$, with τ being the fractional lattice translation, are broken. In such systems, the distinct spin sublattices are linked by rotational or mirror symmetry operations. Since the altermagnetic spin splitting is a

non-relativistic property that manifests without the need for spin-orbit coupling (SOC), the symmetry-theoretical framework should adopt spin space group (SSG) [24–26] although alternative theoretical approaches have been also proposed [27, 28]. An interesting case arises when the symmetry breaking is driven not by a structural distortion generating an effective crystal field on the magnetic ions, but rather by electronic degrees of freedom. This phenomenon occurs in orbitally ordered systems, where an electronic instability leads to the formation of inequivalent sublattices with distinct orbital occupancy patterns [17, 29, 30]. The emergence of the orbitally-ordered state can induce the altermagnetic phase via electronic symmetry breaking, unveiling a hidden altermagnetic phase that remains undetectable through conventional spin-space group analysis [31].

The recent discovery of orbital ordering in the 2D magnetic material VCl_3 [17] presents an ideal platform for exploring coupled orbital and spin phases in low dimensions. Indeed, VCl_3 is part of the vanadium trihalide family, a group of magnetic insulators characterized by their partially filled d -shell [32–39]. In this material, electronic degeneracy and strong on-site correlations on d -manifold lead to electronic symmetry breaking stabilizing an antiferro-orbital (AFO) ground state coexisting with the magnetic order [17] (see Fig. 1). In contrast with the Ising ferromagnet VI_3 [33, 36, 40], where the ferromagnetic coupling is driven by a strong spin-orbit coupling effect [36], VCl_3 it is highly tunable by external perturbations such as substrate interactions [41], stacking configurations [32], and strain [17]. The remarkable tunability of VCl_3 motivates the exploration of the possible coexistence of an antiferromagnetic (AFM) phase coupled with anti-ferro-orbital (AFO) ordering, potentially giving rise to a novel 2D altermagnet [42, 43]. Using a combination of first-principle calculations, model

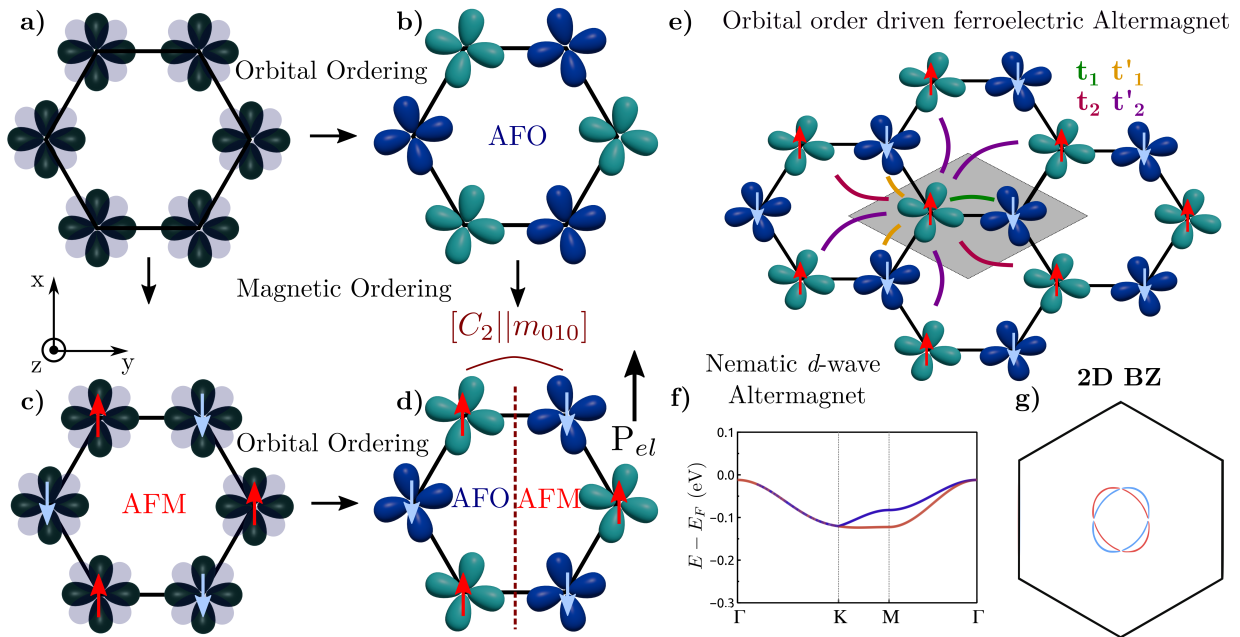


FIG. 1. a) Schematic representation of the high energy phase in honeycomb VCl_3 , highlighting the not ordered in-plane vanadium d -orbitals. b) VCl_3 antiferro-orbital ordering with blue and teal orbitals highlighting the different orbital configuration. In this phase, crystal symmetry are broken by orbital ordering. c) Magnetic ordering on the not ordered phase. d) Single layer VCl_3 showing antiferro-orbital-antiferromagnetic ground state. The opposite spin sublattices are connected via mirror symmetry operation m_{010} . Combining antiferro-orbital ordering with antiferromagnetism give rise to a 2D multiferroic altermagnet. e) Sketch of the two orbital minimal model of AFO-AFM phase with spin-directional hoppings. f) Valence band of the model and in g) energy cut plot in the 2D Brillouin zone highlighting the two nodal lines.

Hamiltonian and symmetry analysis, we demonstrate the emergence of a nematic d -wave ferroelectric switchable altermagnetic phase in monolayer VCl_3 driven by orbital ordering. The multicomponent order originates from the distinctive structural nature of VX_3 compounds characterized by a honeycomb lattice of V cations coordinated by halide ions through edge-sharing distorted octahedra [32–34]. Due to the presence of spin-polarization and orbital degeneracy within a strongly correlated e'_g manifold, the system undergoes spontaneous orbital symmetry breaking, resulting in an orbital-ordered phase (see Fig. 1a-b). The lowest energy state in case of the pristine monolayer is an AFO-ferromagnetic (AFO-FM) phase. We can further tune the magnetic phase by applying strain, inducing an AFO-AFM phase, where compressive strain stabilizes the AFM phase by lowering its energy (see Fig. 1c-d) [17]. In this phase, the two spin sublattices are coupled to the orbital configuration, and, in particular, are connected through a combination of spin flip and mirror operations ($[C_2||m_{010}]$) (see Fig. 1d) [17]. This symmetry creates the conditions for the emergence of an altermagnetic phase. To demonstrate the instrumental role of the AFO-AFM ordering, we construct a minimal tight-binding model on the honeycomb lattice that incorporates all the symmetries to describe the AM

phase:

$$\begin{aligned}
 H_0 = & \beta \sum_i c_i^\dagger (\tau_z \otimes \sigma_z) c_i + \sum_{\langle ij \rangle} t_1(\mathbf{r}_{ij}) c_i^\dagger (\tau_x \otimes \sigma_x) c_j \\
 & + \sum_{\langle\langle ij \rangle\rangle} t_2(\mathbf{r}_{ij}) c_i^\dagger (\mathbf{I} \otimes \mathbf{I}) c_j + h.c.
 \end{aligned} \quad (1)$$

A schematic representation of this two-orbitals model is shown in Fig. 1e, τ and σ matrices describe the sublattice and spin degree of freedoms respectively. The key ingredient responsible of the altermagnetic behavior lies in the directional dependence of the hopping terms. Specifically, the AFO ordering introduces a directional dependence of the hopping due to the different overlap of the d orbitals as given by the Slater-Koster elements [44]. This leads to inequivalent first (t_1 and t'_1) and second (t_2 and t'_2) neighbor hoppings terms (see Fig. 1e). In particular, due to the combination of AFM and AFO orderings, t_2 has both spin and directional dependence (the opposite spins have mirrored hoppings), resulting in a momentum-dependent compensated spin-splitting of the energy bands (see Fig. 1f-g) with energy cuts showing two nodal lines.

Our first-principle calculations on VCl_3 show that the orbital ordering induces a non-relativistic spin splitting (denoted with S) of the bands, as clearly shown in Fig. 2.

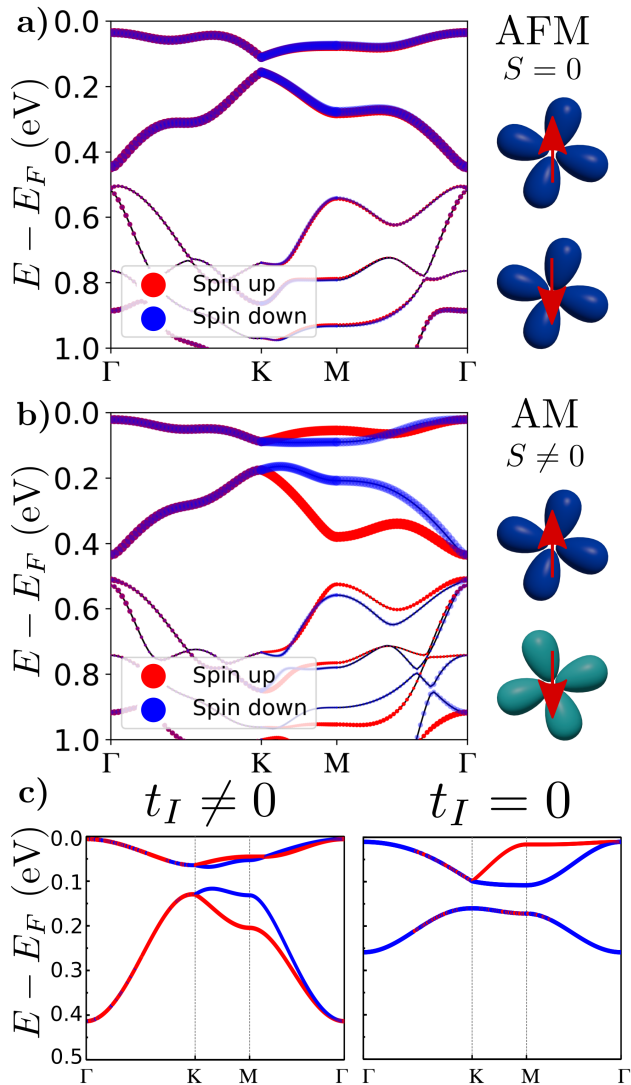


FIG. 2. a) Band structure of the FO-AFM phase, S stands for the AM order parameter. The size of the circles are proportional to the projection of the band structure on vanadium d orbitals. The Fermi level is fixed at the valence band maximum. b) Band structure of the AFO-AFM phase resulting in a 2D altermagnetic phase with an even parity order parameter. c) Band structure of the four orbital model in presence ($t_I \neq 0$) or in absence ($t_I = 0$) of inter-orbital hopping.

In particular, we show the band structure for two different phases considering the lattice in the symmetric D_{3d} structure: FO-AFM and AFO-AFM. In all the orbitally-ordered (OO) phases the system is a semiconductor with a gap of $E_{gap} \sim 2$ eV consistent with recent experimental findings [32, 41] (see supplementary materials (SM) Fig. S1) with the vanadium d -states located at the top of the valence band. The FO ordering (Fig. 2a) combined with an AFM spin state results in an antiferromagnet with degenerate bands due to the presence of time-reversal ($\epsilon_{k,s} \xrightarrow{\mathcal{T}} \epsilon_{-k,-s}$) and inversion symmetry ($\epsilon_{k,s} \xrightarrow{\mathcal{P}} \epsilon_{-k,s}$).

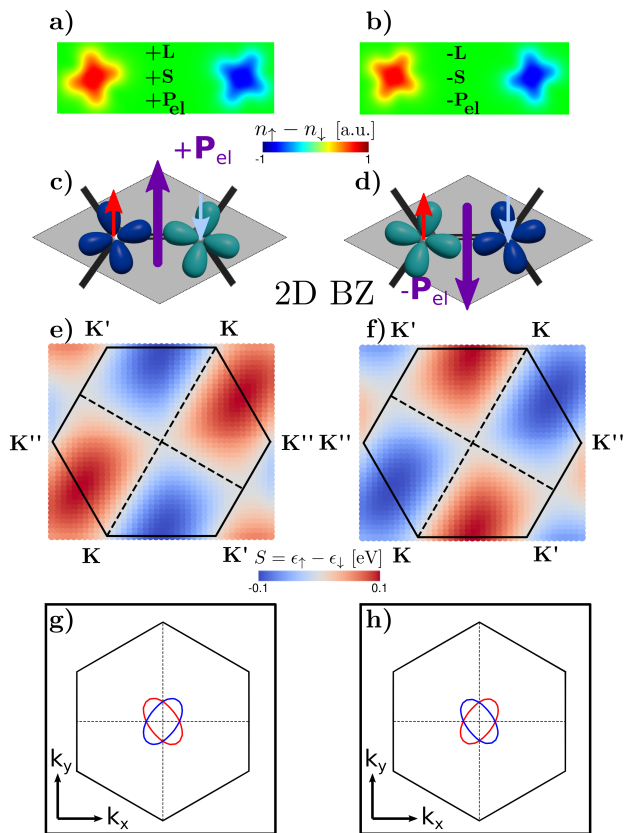


FIG. 3. a) $+L$ electronic configuration. L stands for the orbital configuration, S for the sign of the order parameter and P_{el} is the electronic configuration. b) $-L$ electronic configuration. The arrow points to the direction of the polarization in the xy plane. c) and d) schematics of the different orbital configurations with P_{el} different from zero. e) and f) Corresponding colormap plot of S in the 2D BZ for the $V-d$ conduction state of monolayer VCl_3 . Different K points are present, signalling the presence of different valleys. g) and h) first principle energy cut at the top of the valence band, red for up spin, blue for down spin.

Interestingly, the inversion symmetry breaking [45] induced by AFO ordering in the AFM phase removes degeneracy along some high-symmetry directions of the 2D Brillouin zone (BZ) (see Fig. 2b). The degeneracy along the ΓK is protected by the mirror symmetry operation resulting in an even-parity wave anisotropy of the spin-split bands. By sampling the entire BZ, we find the maximum splitting along the ΓM direction with $\Delta E_k^s \sim 0.2$ eV, which is significant compared to other predicted 2D altermagnets [42]. The two vanadium d -bands exhibit different characteristics: the lower-energy band has predominantly out-of-plane a_{1g} character, while the higher-energy band at the top of the valence band has in-plane e'_g character. As previously discussed, although only the e'_g manifold drives the OO, spin splitting emerges not only in the a_{1g} band but also in $V-d$ and $Cl-p$ hybridized bands below -0.5 eV. This phenomenology can be accounted for by an extended effective model featuring four

orbital, that includes also the a_{1g} - e'_g orbitals (see Fig. 2c and SM for a sketch):

$$H = H_0 + \sum_{\langle ij \rangle, l \neq l'} t_I(\mathbf{r}_{ij}) c_{il}^\dagger (\tau_x \otimes \sigma_x) c_{il} + \mu_{a_{1g}} \sum_i c_{i,a_{1g}}^\dagger c_{i,a_{1g}} \quad (2)$$

where l, l' are the orbitals involved, and $\mu_{a_{1g}}$ is the onsite term for the a_{1g} orbital. In the presence of first neighbor inter-orbital hopping terms, $t_I \neq 0$, spin-splitting also affects the predominantly a_{1g} band, thus accurately capturing the orbital-driven altermagnetic bands observed in the ab-initio calculations. In summary, we have shown how it is possible to stabilize different magnetic orders with different spin splitting driven by orbital and spin order, finding the AFO-AFM phase as an AM.

We now discuss the coupling between electronic and magnetic degrees of freedom, and characterize the symmetries of the AM order parameter. We stabilize two possible orbital configurations, denoted with $+L$ and $-L$, which are characterized by the two distinct AFO orderings (see Fig. 3a-b in which magnetization plots at $z = 0$ are reported). We define $S = \epsilon_\uparrow - \epsilon_\downarrow$ where $\epsilon_{\uparrow(\downarrow)}$ is the single-particle Kohn-Sham eigenvalue for spin up (spin down) and we plot S on a dense k point-mesh ($40 \times 40 \times 1$) in the BZ for V- d conduction band states (see SM Fig. S4 for others V- d states and see Fig. 3e-f). Due to the presence of two nodal lines, we classify VCl_3 as a nematic d -wave AM on a honeycomb lattice. This should be contrasted with the i -wave solution proposed for other 2D AMs with hexagonal BZ [46, 47]. The C_3 symmetry of the honeycomb lattice is now lifted due to the electronic symmetry breaking. Additionally, nematicity emerges due to the further reduction of the C_4 symmetry, typical of d -wave, into C_2 symmetry which is protected by the m_{010} mirror plane. Both the symmetry of spin splitting S and of the isoenergy surfaces at the valence band maximum for the $+L$ and $-L$ case respectively (see Fig. 3g-h), reveal the topology of the AM nodal surface (see Fig. S5 for energy cuts at different energies showing C_2 symmetry). In particular, the sign of S is reversed from K' to K'' , signaling the emergence of different valleys ($K \neq K' \neq K''$) which can be possibly exploited to induce valley-dependent transport and optical effects [48–50] even without SOC (see SM Fig. S6 for the band structure in the different valley and Fig. S7 for the effect of SOC on the band structure).

So far, we have discussed the interplay between electronic, orbital, and spin degrees of freedom within the centrosymmetric structure. However, our OO states are inherently *polar*. This is confirmed by calculating the electronic polarization \mathbf{P}_{ele} for $+L$ and $-L$ orbital-patterns, which exhibit exactly opposite values of $\pm(1.95, 0, 0.02)$ pC/m (see Fig. S8). The polarization lies in the xz plane as dictated by the m_{010} mirror symmetry. Interestingly, the reversal of \mathbf{P}_{ele} is accompanied by the switching of the OO states and the sign

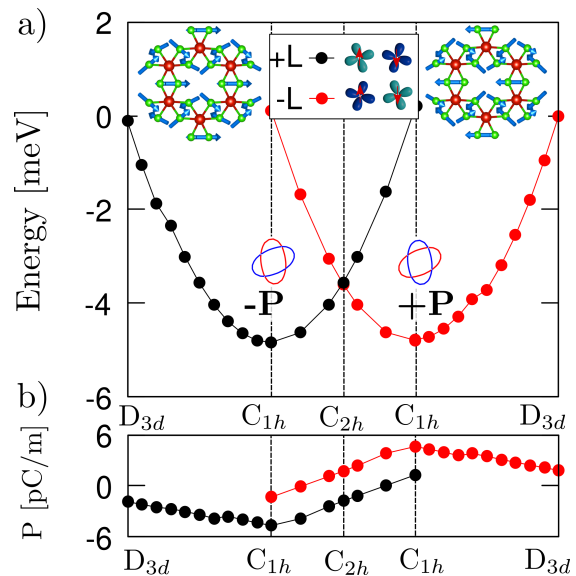


FIG. 4. a) Total energy as a function of the distortion path starting from a D_{3d} symmetry and pointing to the relaxed $+P$ and $-P$ structures. The distortions are reported in the inset. The electronic configuration is fixed at $+L$ (in black) and $-L$ (in red). b) Total polarization as a function of the distortion path.

of the spin-splitting S (see Fig. 3), enabling a coupling between spin-polarized bands and electric polarization. This represents a unique realization of a 2D ferroelectric switchable altermagnet [21] achieved without structural symmetry breaking.

In presence of orbital degeneracy, many-body effects can produce orbital ordering even in the absence of the ionic contribution; this is known as Kugel-Khomskii mechanism [51] and it is recently revisited and applied to altermagnets [30]. However, for real materials, such as KCuF_3 and LaMnO_3 a cooperative Jahn-Teller distortion of the nuclei takes place, and thus the Kugel-Khomskii superexchange alone cannot fully account for their physical properties [52, 53]. For this reason, we now analyze the role of possible structural distortions coupled to the orbital ordering (L), electronic polarization (P_{el}) and non-relativistic spin splitting (S) by means of symmetry broken DFT+ U calculations [39, 54, 55], which allows us to control the occupation tensor [56] during the structural relaxation. We find that the broken symmetry electronic configuration on the symmetric structure (starting from the FO or AFO phases) leads to a slightly structural distortion $|d| \sim 0.07 \text{ \AA}$ of the octahedra due to the non-zero forces on the ions. This reduces the trigonal symmetry $P\bar{3}1m$ (point group D_{3d}) to a monoclinic $C2/m$ (point group C_{2h}) in the case of FO ordering, and a monoclinic Cm (point group C_{1h}) in the case of AFO ordering (see SM for a table with SSG classification). This demonstrated that the orbital polarization induces the structural distortion rather than being its effect. While the combination of mirror symmetry and two-fold rota-

tional axis in $C2/m$ implies centrosymmetry (imposing spin degenerate bands and null polarization), the Cm space group has only a mirror plane symmetry operation generating a nematic d -wave altermagnet. Once the $+L$ ($-L$) is converged in the D_{3d} structure, the system relaxes in the $+P$, $+S$ ($-P$, $-S$) following the distortion shown in the inset of Fig. 4. The energy gain associated with structural relaxation is approximately $\Delta E_{rel} \sim 4.5$ meV/per unit cell, very low compared to typical values in other structural distorted ferroelectric materials [21, 57] but comparable with the ones induced by electronic spin-orientation [58]. In contrast with conventional ferroic materials, where structural distortions primarily remove electronic degeneracy, in our case the electronic configuration drives the distortion. Notably, the $+L$ phase can also be stabilized in the $-P$, $-S$ configuration, albeit at a slightly higher energy (see Fig. 4a) but subsequent ionic relaxation on the $+L$, $-P$, $-S$ phase drives the system in the $+L$, $+P$, $+S$ phase, without entering the $-L$, $+P$, $+S$ phase, further confirming the crucial role of electronic degree of freedom.

Finally, in Fig. 4b we report the polarization as a function of the distortion path. As stated before, in centrosymmetric D_{3d} and C_{2h} structure, there is an electronic contribution to electric polarization, while the ionic one is zero. The relaxation of the ions generates a non zero ionic contribution to the polarization ending up in the relaxed Cm structure where the main contribution is given by P_{ion} (see Fig. S8 in SM for the different contribution to polarization). Interestingly, by a mode decomposition analysis [59–62], we are able disentangle the different contributions to the global distortion and to demonstrate how structural distortion only cause a slight

variation in S thereby confirming the electronic origin of the spin splitting (see SM for further details).

In summary, we demonstrated the emergence of multi-ferroic d -wave altermagnetism in monolayer VCl_3 due a spontaneous orbital order. Our findings, based on first-principles calculations, a model Hamiltonian, and symmetry analysis, show that the interplay between magnetic, electronic, and structural orders induces orbital ordering, making strained monolayer VCl_3 a multiferroic altermagnet. We show that the coupled altermagnetic and ferroelectric orders originate from an electronic symmetry breaking that stabilizes orbital ordering rather than from a structural symmetry as in conventional AM. Our findings unveil a novel framework for identifying 2D altermagnets that are tunable via external factors such as strain and electric fields and simultaneously open new avenues for exploring altermagnetic phases and phenomena in vdW materials.

Acknowledgements- G.P. and A.S. acknowledges financial support by the European Union – NextGenerationEU, Project code PE0000021 - CUP B53C22004060006 - “SUPERMOL”, “Network 4 Energy Sustainable Transition – NEST” and the European Union - NextGenerationEU under the Italian Ministry of University and Research (MUR) National Innovation Ecosystem grant ECS00000041 - VITALITY - CUP E13C22001060006. J.L.L. and A.O.F. acknowledge the computational resources provided by the Aalto Science-IT project and the financial support from the Academy of Finland Projects Nos. 331342, 358088, and 349696, the Jane and Aatos Erkkö Foundation, and the Finnish Quantum Flagship.

-
- [1] Hans Schmid, “Multi-ferroic magnetoelectrics,” *Ferroelectrics* **162**, 317–338 (1994).
- [2] Jeong Min Park, Yuan Cao, Kenji Watanabe, Takashi Taniguchi, and Pablo Jarillo-Herrero, “Tunable strongly coupled superconductivity in magic-angle twisted trilayer graphene,” *Nature* **590**, 249–255 (2021).
- [3] Yuan Cao, Jeong Min Park, Kenji Watanabe, Takashi Taniguchi, and Pablo Jarillo-Herrero, “Pauli-limit violation and re-entrant superconductivity in moiré graphene,” *Nature* **595**, 526–531 (2021).
- [4] Hyunjin Kim, Youngjoon Choi, Cyprian Lewandowski, Alex Thomson, Yiran Zhang, Robert Polski, Kenji Watanabe, Takashi Taniguchi, Jason Alicea, and Stevan Nadj-Perge, “Evidence for unconventional superconductivity in twisted trilayer graphene,” *Nature* **606**, 494–500 (2022).
- [5] Victoria A. Posey, Simon Turkel, Mehdi Rezaee, Aravind Devarakonda, Asish K. Kundu, Chin Shen Ong, Morgan Thinel, Daniel G. Chica, Rocco A. Vitalone, Ran Jing, Suheng Xu, David R. Needell, Elena Meirzadeh, Margalit L. Feuer, Apoorv Jindal, Xiaomeng Cui, Tonica Valla, Patrik Thunström, Turgut Yilmaz, Elio Vescovo, David Graf, Xiaoyang Zhu, Allen Scheie, Andrew F. May, Olle Eriksson, D. N. Basov, Cory R. Dean, Angel Rubio, Philip Kim, Michael E. Ziebel, Andrew J. Millis, Abhay N. Pasupathy, and Xavier Roy, “Two-dimensional heavy fermions in the van der waals metal cesii,” *Nature* **625**, 483–488 (2024).
- [6] Adolfo O. Fumega and Jose L. Lado, “Nature of the unconventional heavy-fermion kondo state in monolayer cesii,” *Nano Letters* **24**, 4272–4278 (2024).
- [7] Arnab Banerjee, Jiaqiang Yan, Johannes Knolle, Craig A. Bridges, Matthew B. Stone, Mark D. Lumsden, David G. Mandrus, David A. Tennant, Roderich Moessner, and Stephen E. Nagler, “Neutron scattering in the proximate quantum spin liquid α -rucl₃,” *Science* **356**, 1055–1059 (2017).
- [8] Stephen M. Winter, Kira Riedl, David Kaib, Radu Coldea, and Roser Valentí, “Probing rucl₃ beyond magnetic order: Effects of temperature and magnetic field,” *Phys. Rev. Lett.* **120**, 077203 (2018).
- [9] Wei Ruan, Yi Chen, Shujie Tang, Jinwoong Hwang, Hsin-Zon Tsai, Ryan L. Lee, Meng Wu, Hyejin Ryu, Salman Kahn, Franklin Liou, Caihong Jia, Andrew Aikawa, Choongyu Hwang, Feng Wang, Yongseong Choi, Steven G. Louie, Patrick A. Lee, Zhi-Xun Shen, Sung-

- Kwan Mo, and Michael F. Crommie, “Evidence for quantum spin liquid behaviour in single-layer $1t\text{-tase2}$ from scanning tunnelling microscopy,” *Nature Physics* **17**, 1154–1161 (2021).
- [10] Quanzhen Zhang, Wen-Yu He, Yu Zhang, Yaoyao Chen, Liangguang Jia, Yanhui Hou, Hongyan Ji, Huixia Yang, Teng Zhang, Liwei Liu, Hong-Jun Gao, Thomas A. Jung, and Yeliang Wang, “Quantum spin liquid signatures in monolayer $1t\text{-nbse2}$,” *Nature Communications* **15** (2024), 10.1038/s41467-024-46612-1.
- [11] Qian Song, Connor A. Occhialini, Emre Ergeçen, Batyr Ilyas, Danila Amoroso, Paolo Barone, Jesse Kapeghian, Kenji Watanabe, Takashi Taniguchi, Antia S. Botana, Silvia Picozzi, Nuh Gedik, and Riccardo Comin, “Evidence for a single-layer van der waals multiferroic,” *Nature* **602**, 601–605 (2022).
- [12] Mohammad Amini, Adolfo O. Fumega, Héctor González-Herrero, Viliam Vaňo, Shawulienu Kezilebieke, Jose L. Lado, and Peter Liljeroth, “Atomic-scale visualization of multiferroicity in monolayer niI2 ,” *Advanced Materials* **36** (2024), 10.1002/adma.202311342.
- [13] Tiancheng Song, Qi-Chao Sun, Eric Anderson, Chong Wang, Jimin Qian, Takashi Taniguchi, Kenji Watanabe, Michael A. McGuire, Rainer Stöhr, Di Xiao, Ting Cao, Jörg Wrachtrup, and Xiaodong Xu, “Direct visualization of magnetic domains and moiré magnetism in twisted 2d magnets,” *Science* **374**, 1140–1144 (2021).
- [14] Hongchao Xie, Xiangpeng Luo, Zhipeng Ye, Zeliang Sun, Gaihua Ye, Suk Hyun Sung, Haiwen Ge, Shaohua Yan, Yang Fu, Shangjie Tian, Hechang Lei, Kai Sun, Robert Hovden, Rui He, and Liuyan Zhao, “Evidence of non-collinear spin texture in magnetic moiré superlattices,” *Nature Physics* **19**, 1150–1155 (2023).
- [15] Adolfo O Fumega and Jose L Lado, “Moiré-driven multiferroic order in twisted crI3 , crBr3 and crI3 bilayers,” *2D Materials* **10**, 025026 (2023).
- [16] Shiva P. Poudel, Juan M. Marmolejo-Tejada, Joseph E. Roll, Martín A. Mosquera, and Salvador Barraza-Lopez, “Creating a three-dimensional intrinsic electric dipole on rotated crI3 bilayers,” *Phys. Rev. B* **107**, 195128 (2023).
- [17] Luigi Camerano, Adolfo O. Fumega, Gianni Profeta, and Jose L. Lado, “Multicomponent magneto-orbital order and magneto-orbitons in monolayer vcl3 ,” *Nano Letters* **0**, null (0).
- [18] Libor Šmejkal, Jairo Sinova, and Tomas Jungwirth, “Beyond conventional ferromagnetism and antiferromagnetism: A phase with nonrelativistic spin and crystal rotation symmetry,” *Physical Review X* **12**, 031042 (2022).
- [19] Igor Mazin and PRX Editors, “Altermagnetism—a new punch line of fundamental magnetism,” (2022).
- [20] Xunkai Duan, Jiayong Zhang, Ziyi Zhu, Yuntian Liu, Zhenyu Zhang, Igor Žutić, and Tong Zhou, “Antiferroelectric altermagnets: Antiferroelectricity alters magnets,” *Phys. Rev. Lett.* **134**, 106801 (2025).
- [21] Mingqiang Gu, Yuntian Liu, Haiyuan Zhu, Kunihiro Yananose, Xiaobing Chen, Yongkang Hu, Alessandro Stroppa, and Qihang Liu, “Ferroelectric switchable altermagnetism,” *Phys. Rev. Lett.* **134**, 106802 (2025).
- [22] Libor Šmejkal, “Altermagnetic multiferroics and altermagnetolectric effect,” arXiv preprint arXiv:2411.19928 (2024).
- [23] Libor Šmejkal, Jairo Sinova, and Tomas Jungwirth, “Emerging research landscape of altermagnetism,” *Physical Review X* **12**, 040501 (2022).
- [24] Pengfei Liu, Jiayu Li, Jingzhi Han, Xiangang Wan, and Qihang Liu, “Spin-group symmetry in magnetic materials with negligible spin-orbit coupling,” *Physical Review X* **12**, 021016 (2022).
- [25] Xiaobing Chen, Jun Ren, Yanzhou Zhu, Yutong Yu, Ao Zhang, Pengfei Liu, Jiayu Li, Yuntian Liu, Caiheng Li, and Qihang Liu, “Enumeration and representation theory of spin space groups,” *Phys. Rev. X* **14**, 031038 (2024).
- [26] Yi Jiang, Ziyin Song, Tiannian Zhu, Zhong Fang, Hongming Weng, Zheng-Xin Liu, Jian Yang, and Chen Fang, “Enumeration of spin-space groups: Toward a complete description of symmetries of magnetic orders,” *Physical Review X* **14**, 031039 (2024).
- [27] Paolo G. Radaelli, “Tensorial approach to altermagnetism,” *Phys. Rev. B* **110**, 214428 (2024).
- [28] Sang-Wook Cheong and Fei-Ting Huang, “Altermagnetism with non-collinear spins,” *npj Quantum Materials* **9** (2024), 10.1038/s41535-024-00626-6.
- [29] Jeroen van den Brink and Daniel I Khomskii, “Multiferroicity due to charge ordering,” *Journal of Physics: Condensed Matter* **20**, 434217 (2008).
- [30] Valentin Leeb, Alexander Mook, Libor Šmejkal, and Johannes Knolle, “Spontaneous formation of altermagnetism from orbital ordering,” *Physical Review Letters* **132** (2024), 10.1103/physrevlett.132.236701.
- [31] Xiaobing Chen, Yuntian Liu, Pengfei Liu, Yutong Yu, J Ren, J Li, A Zhang, and Q Liu, “Catalog of unconventional magnons in collinear magnets,” Preprint at ar-Xiv. <https://doi.org/10.48550/arXiv.2307> (2023).
- [32] Dario Mastrispolito, Luigi Camerano, Hanna Swiatek, Bretislav Smid, Tomasz Klimczuk, Luca Ottaviano, and Gianni Profeta, “Polaronic and mott insulating phase of layered magnetic vanadium trihalide vcl_3 ,” *Phys. Rev. B* **108**, 045126 (2023).
- [33] Tai Kong, Karoline Stolze, Erik I. Timmons, Jing Tao, Danrui Ni, Shu Guo, Zoë Yang, Ruslan Prozorov, and Robert J. Cava, “ Vi3 —a new layered ferromagnetic semiconductor,” *Advanced Materials* **31** (2019), 10.1002/adma.201808074.
- [34] Tai Kong, Shu Guo, Danrui Ni, and Robert J. Cava, “Crystal structure and magnetic properties of the layered van der waals compound VBr_3 ,” *Phys. Rev. Mater.* **3**, 084419 (2019).
- [35] Dávid Hovančík, Jiří Pospíšil, Karel Carva, Vladimír Sechovský, and Cinthia Piamonteze, “Large orbital magnetic moment in vi_3 ,” *Nano Letters* **23**, 1175–1180 (2023).
- [36] Ke Yang, Fengren Fan, Hongbo Wang, D. I. Khomskii, and Hua Wu, “ vi_3 : A two-dimensional ising ferromagnet,” *Phys. Rev. B* **101**, 100402 (2020).
- [37] Alessandro De Vita, Thao Thi Phuong Nguyen, Roberto Sant, Gian Marco Pierantozzi, Danila Amoroso, Chiara Bigi, Vincent Polewczyk, Giovanni Vinai, Loi T. Nguyen, Tai Kong, Jun Fujii, Ivana Vobornik, Nicholas B. Brookes, Giorgio Rossi, Robert J. Cava, Federico Mazzola, Kunihiko Yamauchi, Silvia Picozzi, and Giancarlo Panaccione, “Influence of orbital character on the ground state electronic properties in the van der waals transition metal iodides vi_3 and crI3 ,” *Nano Letters* **22**, 7034–7041 (2022).
- [38] Derek Bergner, Tai Kong, Ping Ai, Daniel Eilbott,

- Claudia Fatuzzo, Samuel Ciocys, Nicholas Dale, Conrad Stansbury, Drew W. Latzke, Everardo Molina, Ryan Reno, Robert J. Cava, Alessandra Lanzara, and Claudia Ojeda-Aristizabal, “Polarization dependent photoemission as a probe of the magnetic ground state in the van der waals ferromagnet vi_3 ,” *Applied Physics Letters* **121** (2022), 10.1063/5.0108498.
- [39] Luigi Camerano and Gianni Profeta, “Symmetry breaking in vanadium trihalides,” *2D Materials* **11**, 025027 (2024).
- [40] I. V. Solovyev, R. Ono, and S. A. Nikolaev, “Ferromagnetic ferroelectricity due to the kugel-khonskii mechanism of orbital ordering assisted by atomic hund’s second rule effects,” *Phys. Rev. B* **110**, 205116 (2024).
- [41] Jinghao Deng, Deping Guo, Yao Wen, Shuangzan Lu, Zhengbo Cheng, Zemin Pan, Tao Jian, Yusong Bai, Hui Zhang, Wei Ji, Jun He, and Chendong Zhang, “Ferroelectricity in an antiferromagnetic vanadium trichloride monolayer,” (2024).
- [42] Joachim Sodequist and Thomas Olsen, “Two-dimensional altermagnets from high throughput computational screening: Symmetry requirements, chiral magnons, and spin-orbit effects,” *Applied Physics Letters* **124** (2024).
- [43] Sike Zeng and Yu-Jun Zhao, “Description of two-dimensional altermagnetism: Categorization using spin group theory,” *Phys. Rev. B* **110**, 054406 (2024).
- [44] J. C. Slater and G. F. Koster, “Simplified lcao method for the periodic potential problem,” *Phys. Rev.* **94**, 1498–1524 (1954).
- [45] Note that there is a finite thickness of VCl_3 monolayer.
- [46] Sike Zeng and Yu-Jun Zhao, “Description of two-dimensional altermagnetism: Categorization using spin group theory,” *Phys. Rev. B* **110**, 054406 (2024).
- [47] Sike Zeng and Yu-Jun Zhao, “Bilayer stacking a -type altermagnet: A general approach to generating two-dimensional altermagnetism,” *Phys. Rev. B* **110**, 174410 (2024).
- [48] Yuya Ominato, Junji Fujimoto, and Mamoru Matsuo, “Valley-dependent spin transport in monolayer transition-metal dichalcogenides,” *Phys. Rev. Lett.* **124**, 166803 (2020).
- [49] Takehito Yokoyama, “Controllable valley and spin transport in ferromagnetic silicene junctions,” *Phys. Rev. B* **87**, 241409 (2013).
- [50] Domenico Di Sante, Alessandro Stroppa, Paolo Barone, Myung-Hwan Whangbo, and Silvia Picozzi, “Emergence of ferroelectricity and spin-valley properties in two-dimensional honeycomb binary compounds,” *Phys. Rev. B* **91**, 161401 (2015).
- [51] “Crystal-structure and magnetic properties of substances with orbital degeneracy,” *Zh. Eksp. Teor. Fiz* **64**, 1429–1439 (1973).
- [52] E. Pavarini, E. Koch, and A. I. Lichtenstein, “Mechanism for orbital ordering in ku_3f_3 ,” *Phys. Rev. Lett.* **101**, 266405 (2008).
- [53] Eva Pavarini and Erik Koch, “Origin of jahn-teller distortion and orbital order in lamno_3 ,” *Phys. Rev. Lett.* **104**, 086402 (2010).
- [54] Alex Zunger, “Bridging the gap between density functional theory and quantum materials,” *Nature Computational Science* **2**, 529–532 (2022).
- [55] Oleksandr I Malyi and Alex Zunger, “False metals, real insulators, and degenerate gapped metals,” *Applied Physics Reviews* **7**, 041310 (2020).
- [56] Jeremy P. Allen and Graeme W. Watson, “Occupation matrix control of d- and f-electron localisations using dft + u,” *Phys. Chem. Chem. Phys.* **16**, 21016–21031 (2014).
- [57] Alessandro Stroppa, Paolo Barone, Prashant Jain, Jean Manuel Perez-Mato, and Silvia Picozzi, “Hybrid improper ferroelectricity in a multiferroic and magnetoelectric metal-organic framework,” *Advanced Materials* **25**, 2284–2290 (2013).
- [58] Silvia Picozzi, Kunihiko Yamauchi, Biplab Sanyal, Ivan A Sergienko, and Elbio Dagotto, “Dual nature of improper ferroelectricity in a magnetoelectric multiferroic,” *Physical Review Letters* **99**, 227201 (2007).
- [59] Mois Iliia Aroyo, Juan Manuel Perez-Mato, Cesar Capillas, Eli Kroumova, Svetoslav Ivantchev, Gotzon Madariaga, Asen Kirov, and Hans Wondratschek, “Bilbao crystallographic server: I. databases and crystallographic computing programs,” *Zeitschrift für Kristallographie - Crystalline Materials* **221**, 15–27 (2006).
- [60] Mois I. Aroyo, Asen Kirov, Cesar Capillas, J. M. Perez-Mato, and Hans Wondratschek, “Bilbao crystallographic server. ii. representations of crystallographic point groups and space groups,” *Acta Crystallographica Section A Foundations of Crystallography* **62**, 115–128 (2006).
- [61] E. Kroumova, M. I. Aroyo, J. M. Perez-Mato, S. Ivantchev, J. M. Igartua, and H. Wondratschek, “Pseudo: a program for a pseudosymmetry search,” *Journal of Applied Crystallography* **34**, 783–784 (2001).
- [62] Asen K. Kirov, Mois I. Aroyo, and J. Manuel Perez-Mato, “Neutron: a program for computing phonon extinction rules of inelastic neutron scattering and thermal diffuse scattering experiments,” *Journal of Applied Crystallography* **36**, 1085–1089 (2003).

Supplemental material and supporting information for

Multiferroic nematic d -wave altermagnetism driven by orbital-order on the honeycomb lattice

Luigi Camerano^a, Adolfo O. Fumega^b, Jose L. Lado^b, Alessandro Stroppa^c, Gianni Profeta^{a,c}

^a Department of Physical and Chemical Sciences, University of L'Aquila, Via Vetoio 67100 L'Aquila, Italy

^b Department of Applied Physics, Aalto University, 02150 Espoo, Finland

^c CNR-SPIN L'Aquila, Via Vetoio, 67100 L'Aquila, Italy *c/o* Department of Physical and Chemical Sciences, University of L'Aquila, Via Vetoio, 67100 L'Aquila, Italy

CONTENTS

I. Methods	2
II. Supplementary Figures	2
A. Energy gap in monolayer VCl_3	2
B. Altermagnetic models on the honeycomb lattice	3
C. Symmetry of the altermagnetic spin splitting	5
D. Polarization and mode decomposition analysis	7
References	10

I. METHODS

Density functional theory calculations were performed using the Vienna ab-initio Simulation Package (VASP) [1, 2], using both the generalized gradient approximation (GGA), in the Perdew-Burke-Ernzerhof (PBE) parametrization for the exchange-correlation functional [3]. Interactions between electrons and nuclei were described using the projector-augmented wave method. Energy thresholds for the self-consistent calculation was set to 10^{-7} eV and force threshold for geometry optimization 10^{-5} eV \AA^{-1} . A plane-wave kinetic energy cutoff of 500 eV was employed for VCl_3 . The Brillouin zone was sampled using a $12 \times 12 \times 1$ Gamma-centered Monkhorst-Pack grid. To account for the on-site electron-electron correlation we used the GGA+U. The linear response effective Hubbard term U calculated by Ref. [4] is $U = 3.27$ eV. The precondition on the on-site d -density matrix was set using the method explained in Refs. [5, 6].

II. SUPPLEMENTARY FIGURES

A. Energy gap in monolayer VCl_3

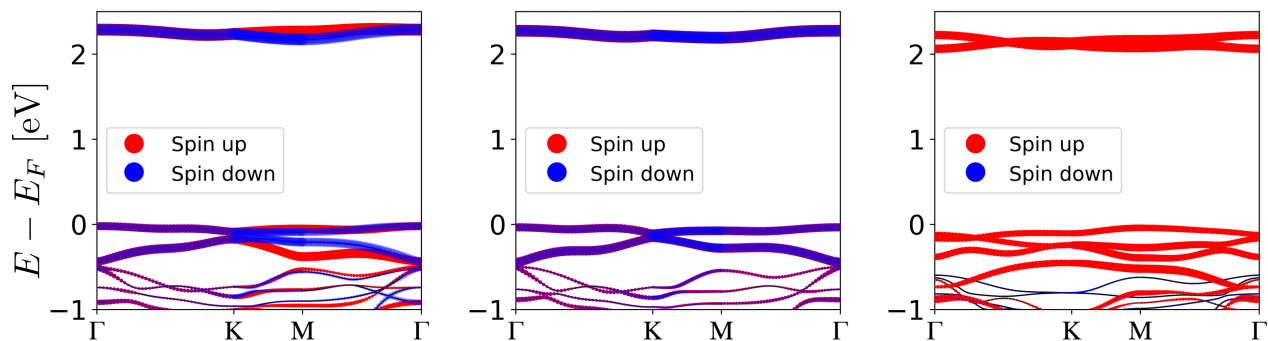


FIG. S1. From left to right: band structure of AM, AFM, FM phases (see main manuscript) showing the gap opening between V- d orbitals. The point size in the plots is proportional to the projection on V- d orbitals

B. Altermagnetic models on the honeycomb lattice

In this section we will briefly discuss altermagnetic models on the honeycomb lattice. As discussed in the manuscript, the minimal model H_0 showing a nematic d -wave spin splitting is a two orbital model with spin-directional second nearest neighbors hoppings whose values (in eV) are reported in Tab. S1.

The minimal model can be extended by introducing the Hamiltonian H of the main manuscript, thus including

t_1	t'_1	t_2	t'_2	β
0.05	0.03	0.02	0.01	0.5

TABLE S1. TB parameter for the two orbital model

the a_{1g} orbital. The sketch of this four orbital model is reported in Fig. S2. As soon as the inter-orbital hopping is different from zero $t_I \neq 0$, spin-splitting involves also a_{1g} band (see Tab.S2 for the parameters of the model in eV). Note that in these two models orbital ordering determines the directionality dependence of the hoppings. To

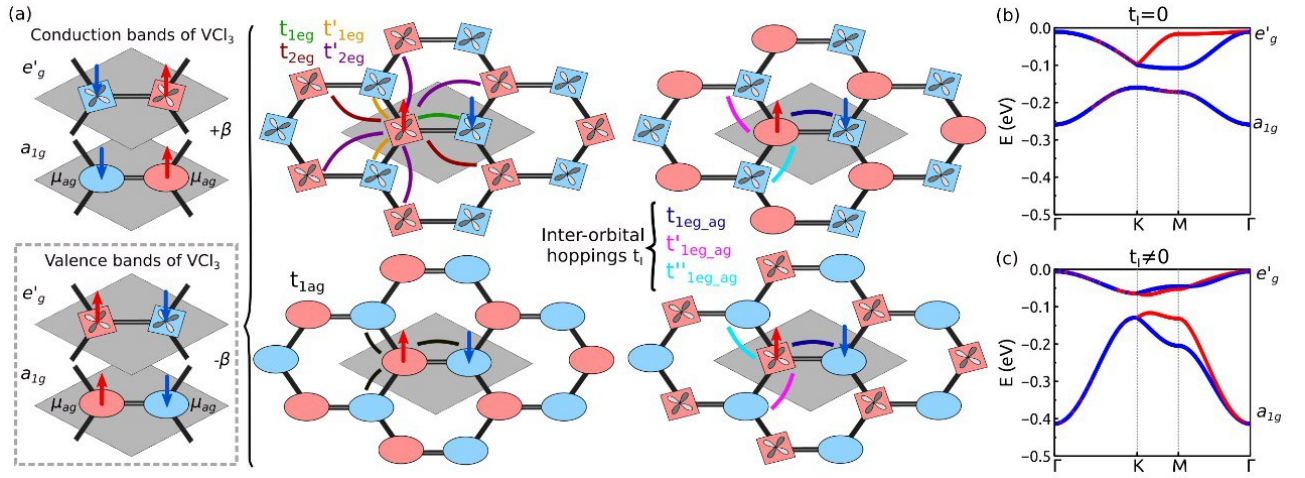


FIG. S2. Sketch of the four orbital model including a_{1g} and e'_g orbitals.

t_{1,e'_g}	t'_{1,e'_g}	$t_{1,a_{1g}}$	$t_{1,e'_g a_{1g}}$	$t'_{1,e'_g a_{1g}}$	$t''_{1,e'_g a_{1g}}$	t_{2,e'_g}	t'_{2,e'_g}	β	$\mu_{a_{1g}}$
0.010	0.100	0.110	0.130	0.290	0.050	0.029	0.006	0.5	-0.11

TABLE S2. TB parameter for the four orbital $a_{1g}e'_g$ model

explicitly include the orbital configuration in the model we build up a minimal four orbital, H_{OO} , for the e'_g manifold. Introducing an α parameter that impose the orbital configuration we can write:

$$H_{OO} = \alpha \sum_{i,l,s} (-1)^l \mathbf{c}_{ils}^\dagger \hat{\tau}_z \mathbf{c}_{ils} + \beta \sum_{i,l,s} \sigma_{ss}^z \mathbf{c}_{ils}^\dagger \hat{\tau}_z \mathbf{c}_{ils} + \sum_{ij,kl,s} t(\mathbf{r}_{il,jk}) \mathbf{c}_{ils}^\dagger (\hat{\mathbf{I}} + \hat{\tau}_x) \mathbf{c}_{jks} + h.c. \quad (1)$$

where τ and σ matrices describe the sublattice and spin degree of freedoms. A sketch of this model is reported in Fig. S3. Here, by playing with the α parameter both $+L$ and $-L$ configuration can be obtained. For $\alpha = 0$ orbital ordering is quenched and a non-altermagnetic solution arises.

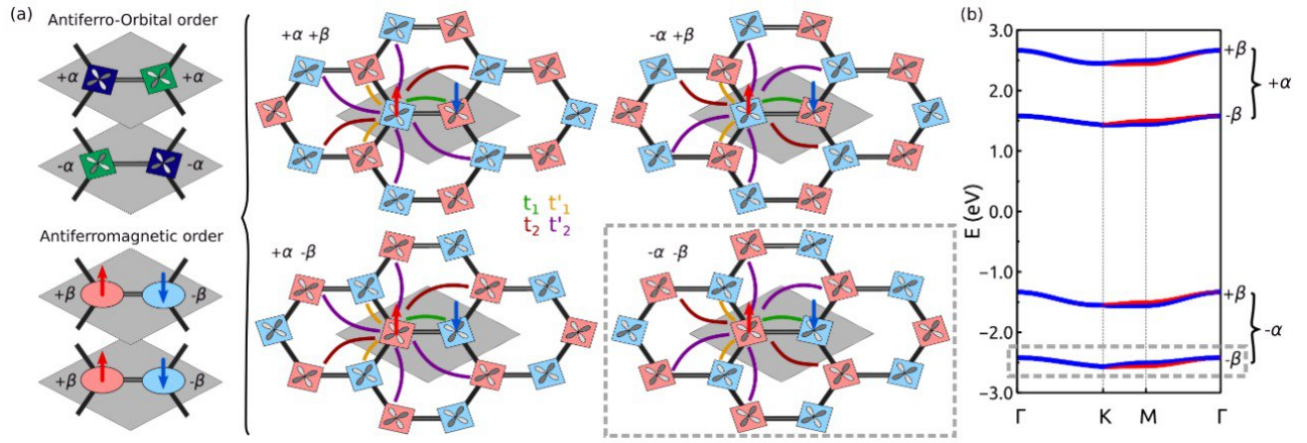


FIG. S3. Sketch of the four orbital model including the e'_g manifold.

C. Symmetry of the altermagnetic spin splitting

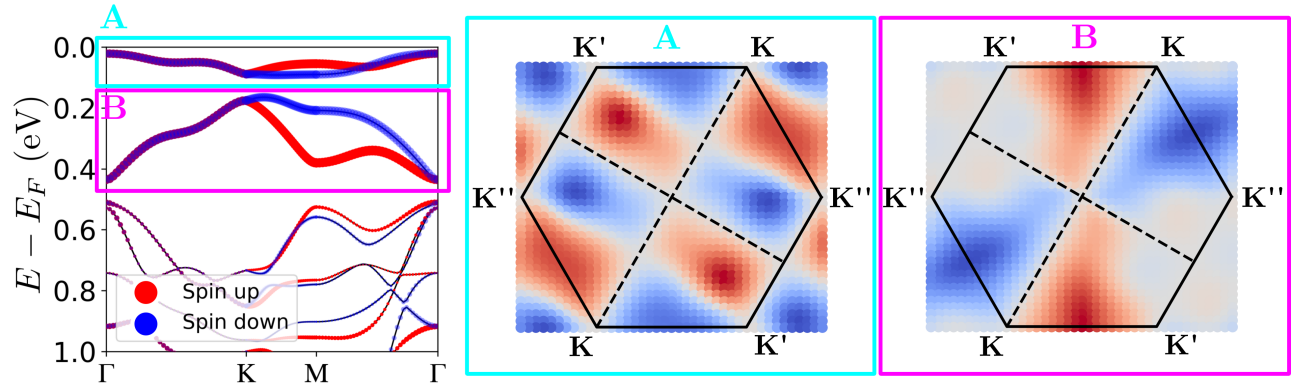


FIG. S4. The defined parameter S (see main manuscript) for different valence bands. In particular, S for the highlighted region (in cyan and magenta) reported in the left panel is reported in center and right panel respectively showing the same d -wave symmetry.

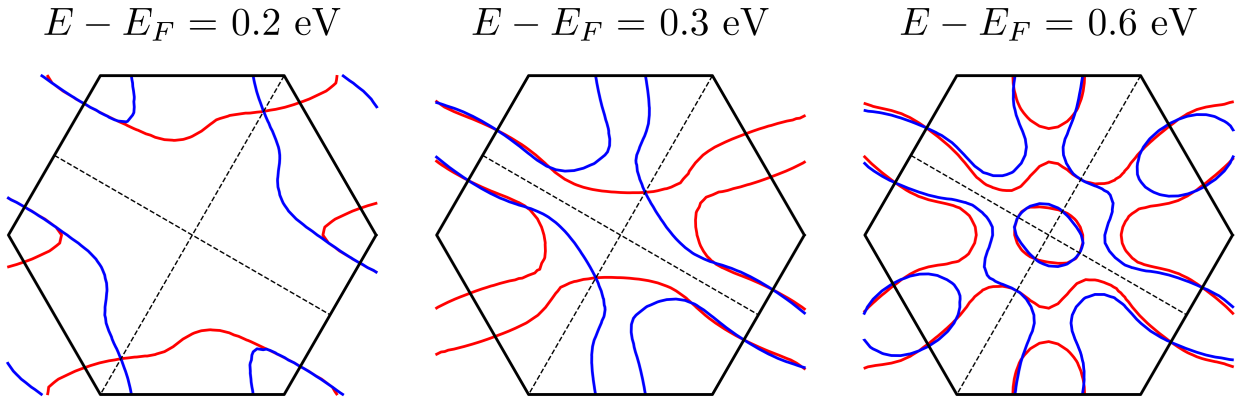


FIG. S5. a) Energy cuts at different energies showing the symmetry of AM order parameter. In particular, it is clear that C_4 symmetry is broken resulting in a nematic d -wave altermagnet.

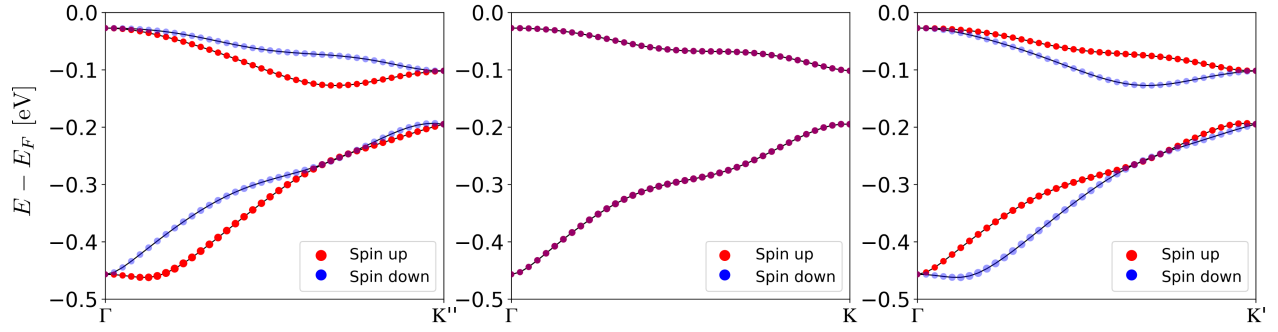


FIG. S6. V- d projected band structure along inequivalent K points in the 2D BZ showing a spin-valley locking in absence of SOC.

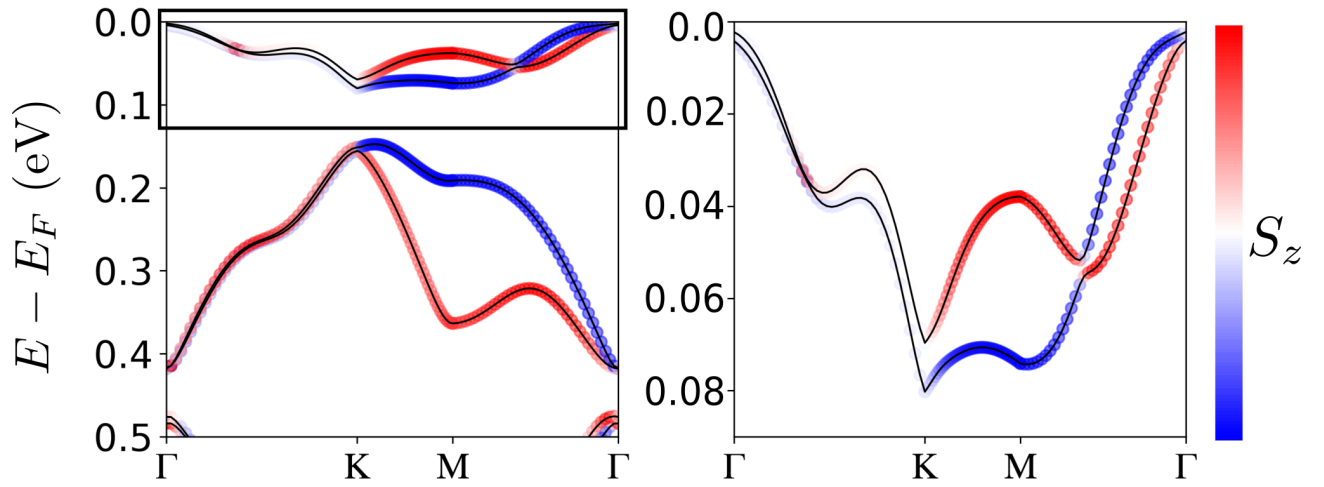


FIG. S7. Effect of spin-orbit coupling on the V- d valence bands showing a minimal modification of the bands.

D. Polarization and mode decomposition analysis

In this section we use a symmetry mode decomposition analysis (using the Pseudosymmetry [7] and Amplitudes [8] tools of the Bilbao Crystallographic server [9, 10]) to decouple the contribution of different modes on the energy gain, ionic and electronic polarization and spin splitting S . Starting from a $P\bar{3}1m$ structure, our symmetry analysis detects 3 modes: the non-polar Γ_3^+ ($|d| \sim 0.06$ Å) and the polar Γ_3^- ($|d| \sim 0.02$ Å) and Γ_2^- ($|d| \sim 0.002$ Å). The latter is very small and has not effect on the total energy, polarization and S within our numerical tolerance. In Fig. S7 we report ionic displacement for the Γ_3^+ and Γ_3^- , while in Fig. S8 total energy curves show energy gain and the distinct ionic and electronic contribution to the polarization. As expected, while Γ_3^+ does not contribute to ionic polarization, Γ_3^- gives rise to an additional ionic contribution to the polarization. Regarding the electronic structure configuration, in Fig. S9 we report band structure for the different distortion modes, independently, and the associated S value. Notably, structural distortion has little effect on the energy bands, causing only slight variations in S and thereby confirming the electronic origin of the spin splitting.

Space Group	Magnetic Space Group	Spin Group	Spin Splitting
$P\bar{3}1m$	$P\bar{3}'1m$	$P^{-1}\bar{3}1^{-1}m^{\infty m}1$	No
$C2/m$	$C2'/m$	$C^12/^{-1}m^{\infty m}1$	No
Cm	Cm	$C^{-1}m^{\infty m}1$	Yes

TABLE S3. Tables of Space Group, Magnetic Space Group, Spin Group and Spin Splitting for the mode decomposition in monolayer VCl_3

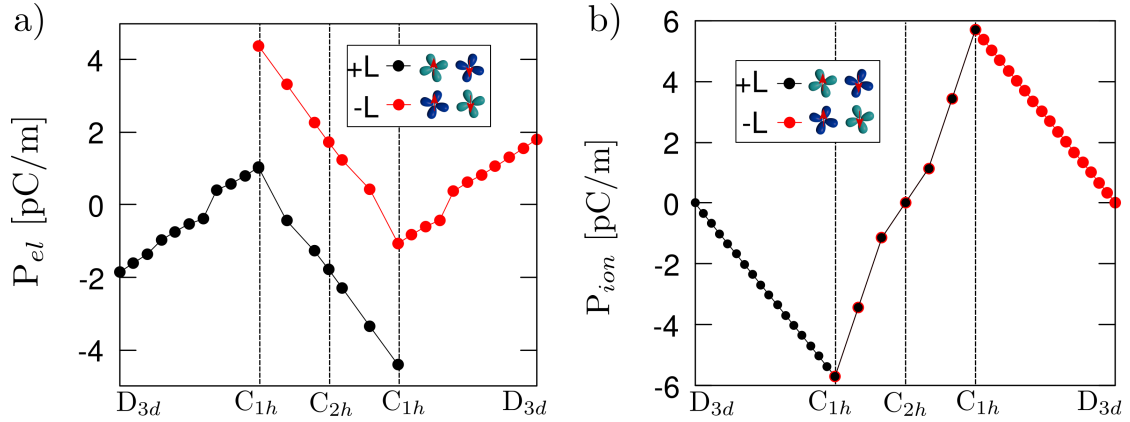


FIG. S8. a) Electronic polarization as P_{el} as a function of the distortion path. b) Ionic polarization as P_{ion} as a function of the distortion path. The polarization for monolayer VCl_3 is reported in pC/m following the convention for 2D materials.

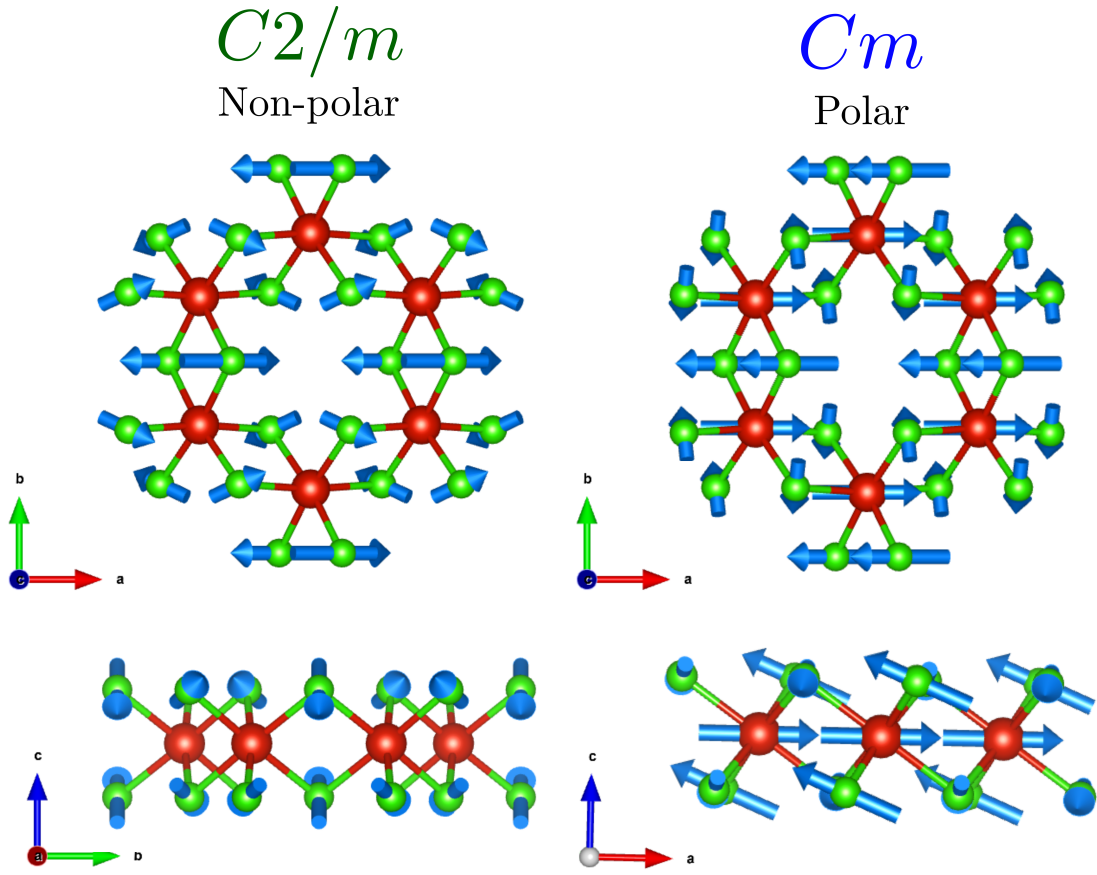


FIG. S9. Left panel: distortion $C2/m$ non-polar mode mainly involving the halides. Right panel: distortive Cm polar mode including both V and Cl.

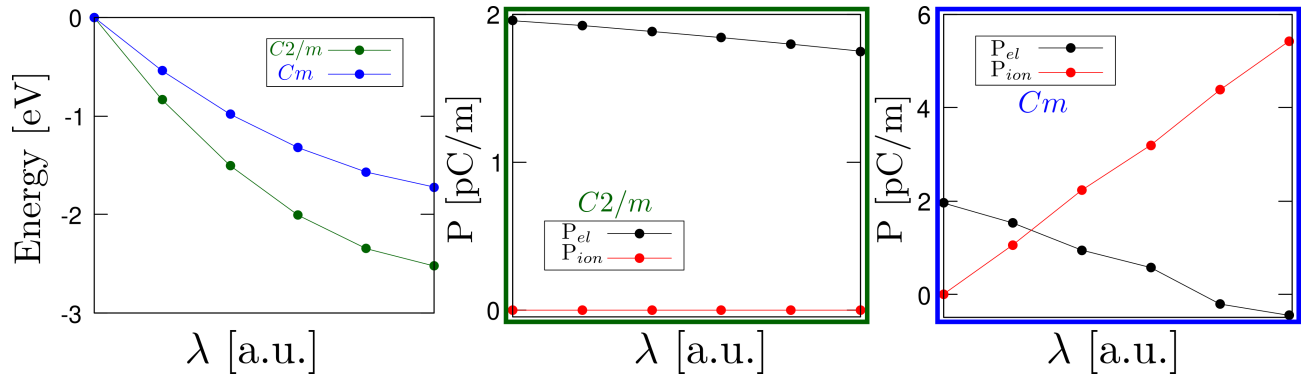


FIG. S10. Left panel: energy as a function of the displacement for the different modes active (see the main text). Following both of the modes decrease the energy of the system. Center panel: electronic and ionic polarization for the $C2/m$ mode. Since it is a non-polar mode, ionic polarization is zero. Right panel: as expected this polar mode activates the ionic polarization. Electronic polarization is different from zero for both the cases.

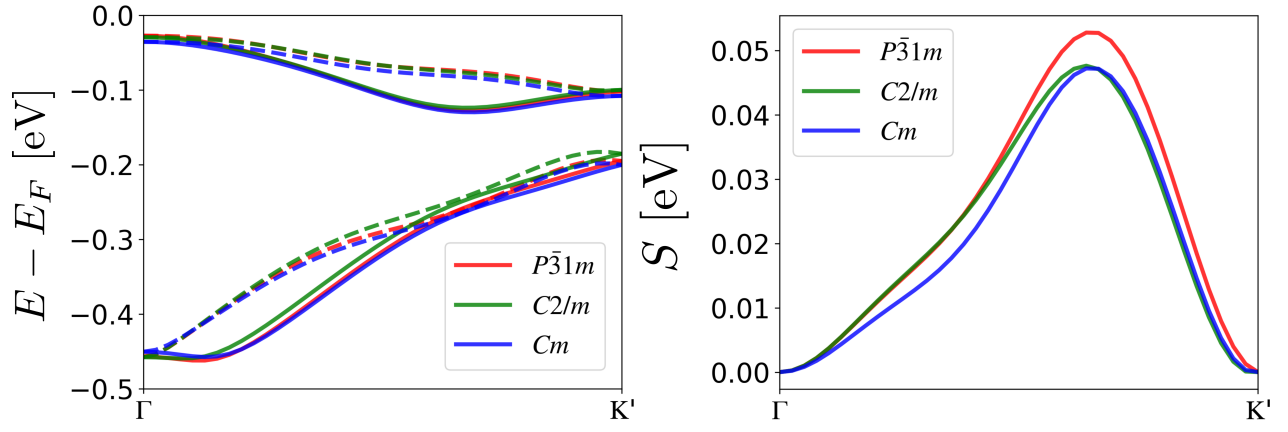


FIG. S11. Left panel: band structure for the different modes end points. The straight (dashed) line is for spin up (spin down). Right panel: the sign of S along the $\Gamma K'$ line, showing the negligible influence of the distortion modes on the spin-splitting S .

-
- [1] G. Kresse and J. Hafner, “Ab initio molecular dynamics for liquid metals,” *Phys. Rev. B* **47**, 558–561 (1993).
 - [2] G. Kresse and D. Joubert, “From ultrasoft pseudopotentials to the projector augmented-wave method,” *Phys. Rev. B* **59**, 1758–1775 (1999).
 - [3] John P. Perdew, Kieron Burke, and Matthias Ernzerhof, “Generalized gradient approximation made simple,” *Phys. Rev. Lett.* **77**, 3865–3868 (1996).
 - [4] Junjie He, Shuangying Ma, Pengbo Lyu, and Petr Nachtigall, “Unusual dirac half-metallicity with intrinsic ferromagnetism in vanadium trihalide monolayers,” *Journal of Materials Chemistry C* **4**, 2518–2526 (2016).
 - [5] Luigi Camerano and Gianni Profeta, “Symmetry breaking in vanadium trihalides,” *2D Materials* **11**, 025027 (2024).
 - [6] Jeremy P. Allen and Graeme W. Watson, “Occupation matrix control of d- and f-electron localisations using dft + u,” *Phys. Chem. Chem. Phys.* **16**, 21016–21031 (2014).
 - [7] E. Kroumova, M. I. Aroyo, J. M. Perez-Mato, S. Ivantchev, J. M. Igartua, and H. Wondratschek, “Pseudo: a program for a pseudosymmetry search,” *Journal of Applied Crystallography* **34**, 783–784 (2001).
 - [8] Asen K. Kirov, Mois I. Aroyo, and J. Manuel Perez-Mato, “Neutron: a program for computing phonon extinction rules of inelastic neutron scattering and thermal diffuse scattering experiments,” *Journal of Applied Crystallography* **36**, 1085–1089 (2003).
 - [9] Mois Ilia Aroyo, Juan Manuel Perez-Mato, Cesar Capillas, Eli Kroumova, Svetoslav Ivantchev, Gotzon Madariaga, Asen Kirov, and Hans Wondratschek, “Bilbao crystallographic server: I. databases and crystallographic computing programs,” *Zeitschrift für Kristallographie - Crystalline Materials* **221**, 15–27 (2006).
 - [10] Mois I. Aroyo, Asen Kirov, Cesar Capillas, J. M. Perez-Mato, and Hans Wondratschek, “Bilbao crystallographic server. ii. representations of crystallographic point groups and space groups,” *Acta Crystallographica Section A Foundations of Crystallography* **62**, 115–128 (2006).